Bahraq *et al. Int J Concr Struct Mater* (2019) 13:6
https://doi.org/10.1186/s40069-018-0330-z

International Journal of Concrete Structures and Materials

ORIGINAL ARTICLE Open Access

Experimental and Numerical Investigation of Shear Behavior of RC Beams Strengthened by Ultra-High Performance Concrete

Ashraf Awadh Bahraq[1], Mohammed Ali Al-Osta[1*], Shamsad Ahmad[1], Mesfer Mohammad Al-Zahrani[1], Salah Othman Al-Dulaijan[1] and Muhammad Kalimur Rahman[2]

Abstract

This paper presents a study on the shear behavior of reinforced concrete (RC) beams strengthened by jacketing the surfaces of the beams using ultra-high performance fiber reinforced concrete (UHPC). The surfaces of the RC beams were prepared by sandblasting and UHPC was cast in situ over the surfaces of RC beams. The beams were strengthened using two different strengthening configurations; (i) two longitudinal sides strengthening (ii) three sides strengthening. The bond between normal concrete and UHPC was examined by conducting splitting tensile strength and slant shear strength tests on composite cylindrical specimens cast using normal concrete and UHPC. The control and strengthened beam specimens were tested using four-point loading arrangement maintaining different shear span-to-depth ratios. The results of tested beams showed the beneficial effects of strengthening the RC beams using UHPC, as evident from enhancement of the shear capacity and shifting of the failure mode from brittle to ductile with more stiff behavior. In addition, a non-linear finite element model (FEM) was developed to examine the sufficiency of the experimental results used to study the shear behavior of control and strengthened beams. The failure loads and the crack patterns determined experimentally matched well with those predicted using the proposed model with a reasonably good degree of accuracy.

Keywords: RC beam, shear behavior, strengthening, ultra-high performance fiber reinforced concrete, bond strength, finite element model

1 Background

Concrete structures need repairing or strengthening when they have some deficiencies in their structural performance and/or durability properties. Such deficiencies could be due to many reasons such as errors in deign calculations or construction practices; unexpected increasing in loads; change in service conditions; deteriorations resulting from corrosion of steel rebars or other chemical attacks, etc. As far as structural performance is concerned, both flexural and shear strengths requirements should be satisfied. RC members are mainly designed to develop their full strength (Altin et al. 2005). However, in some cases the failure of beams can take place due to deficiency in the design for shear. Since the shear failure occurs suddenly and may lead to catastrophic consequences, the necessity of the adequate shear capacity of RC beams should be given due importance. Accordingly, researches pertaining to strengthening the RC beams deficient in shear are reported.

Ultra-high performance concrete (UHPC), which is a hybrid of the cementitious materials and high-tensile strength steel fibers, can be used to strengthen the RC members (Al-osta 2018). UHPC is reported to have outstanding properties such as ultra-high strength, good flowability, excellent ductility, high serviceability, high strength-to-weight ratio, aesthetically appearance through self-levelling property, and overall superior durability properties such as low permeability and highly

*Correspondence: malosta@kfupm.edu.sa
[1] Civil & Environmental Engineering Department, King Fahd University of Petroleum & Minerals, Dhahran 31261, Saudi Arabia
Full list of author information is available at the end of the article
Journal information: ISSN 1976-0485 / eISSN 2234-1315

resistant against reinforcement corrosion (Ahmad et al. 2015). Moreover, the UHPC can effectively be bonded with the sandblasted surfaces of existing old reinforced structures and thus making it suitable for rehabilitation and strengthening of RC structures (Martinola et al. 2010; Al-Osta et al. 2017).

UHPC strengthening system is an alternative approach to rehabilitate or restore the deteriorated concrete members or to retrofit or strengthen the sound concrete members. It has exceptional advantages over traditional methods such as steel plate-bonding (Altin et al. 2005), fiber reinforced polymer (FRP) strengthening (Chen and Teng 2003), section enlargement, etc. For example, FRP possesses desired properties such as high strength, corrosion resistance, ease to apply, and without much change in the size of the structural member. However, FRP system has some shortcomings, which are mainly related to bonding, compatibility and fire-resistance problems. On the other hand, UHPC can be used as a strengthening material for existing structures having either sound or deteriorated concrete surfaces. Therefore, for repairing or rehabilitating of concrete structures, UHPC can be considered as a good option which can enhance the structural performance and durability of substrate concrete (Li 2004).

Throughout the last decade, an attempt was made by various researchers to use the high strength concretes, generally the steel fiber reinforced concrete, for purposes of structural strengthening. The flexural and shear behavior of the RC beams retrofitted using high-performance fiber reinforced concrete (HPFRC) was studied by Alaee et al. (2003). The results of this study indicated the feasibility of using HPFRC for upgrading the flexural and shear capacities of member as well as enhancing the durability properties through the dense mixture of such concrete. Farhat et al. (2007) investigated the behavior of damaged beams strengthened using the high-performance fiber reinforced cementitious composite (HPFRCC). The results showed that if the strengthening is done by applying HPFRCC on the tension face as well as on the side faces, the failure load would increase up to 86%. The strengthening technique using a 40 mm layer of high performance fiber reinforced concrete (HPFRC) was experimentally and numerically studied by Martinola et al. (2010). The results showed that the use of HPFRC jacketing for strengthening has a significant effect in increasing the load carrying capacity by a factor of 2.15. Furthermore, a good enhancement in the durability of the beams was observed due to use of HPFRC jacketing. Noshiravani and Brühwiler (2013) experimentally investigated the composite section made of RC and UHPC. This study concluded that a layer of UHPC applied at the tensile face could be used as an effective shear strengthening. Bastiien-Masse and Brühwiler (2014) investigated the structural behavior of the beams and slabs retrofitted using UHPC. Composite beams and slabs, which included 50 mm thick layer of UHPC were prepared and tested under different types of loading. The results clearly demonstrated that the use of UHPC layer over RC section had an effective enhancement on the load bearing capacity. Ruano et al. (2015) reported the shear behavior of RC beams retrofitted using steel fiber reinforced concrete (SFRC). The results indicated that the presence of fiber prevents debonding and generally enhances overall integrity of the beams. Chalioris et al. (2014) investigated the use of thin reinforced self-compacting concrete for strengthening of conventional RC beams. The results showed an increase in the strength with improvement in the ductility and favorable failure behavior. Hussein and Amleh (2015) evaluated the flexural and shear capacities of beams made with UHPC-normal strength concrete composite without stirrups. The results showed that such composite technique improved the performance of members strengthened in flexure and shear. The benefits of using UHPC for strengthening of conventional RC beams was demonstrated by Lampropoulos et al. (2016). Different configurations of UHPC layers used for strengthening consisted of jacketing of tensile face alone, compressive face alone, and three-side jacketing. A significant increase in the moment capacity was observed in case of UHPC jacketing from three sides. The flexural behavior of strengthened conventional RC beams using UHPC was experimentally studied by Al-Osta et al. (2017). The results showed that the proposed strengthening technique was enhanced the structural performance of retrofitted beams through increasing flexural capacity and overall stiffness.

Various studies are reported about use of finite element modelling for studying the shear behavior of strengthened beams including prediction of failure loads and cracking patterns. However, the modelling of concrete cracking is the most challenging task. Lampropoulos et al. (2016) used the smeared crack approach in the analysis of strengthened beams. Concrete damage plasticity model is most commonly used for simulation of the cracking in concrete (Al-Osta et al. 2017). Al-Osta et al. (2017) developed a finite element model of strengthened beams in flexural using the concrete damage plasticity theory and they found that their proposed model predicted the load–deflection response and the crack patterns in good agreement with the experimental results.

Despite the above mentioned research works pertaining to the use of UHPC in strengthening of RC beams, it can be observed that limited works had considered the jacketing by applying the UHPC along the vertical sides. In addition, there is a lack of information about the effect

of UHPC jacketing on the shear behavior of strengthened RC beams. In addition, the effect of the shear span-to-depth ratio on the behavior of strengthened RC beams was not investigated. Consequently, in this research work, the behavior of two different configurations for strengthening of RC beams using UHPC is investigated experimentally. Additionally, a numerical model is developed to validate the experimental results. Moreover, the failure behavior of the non-strengthened and strengthened RC beams was studied considering the experimental variables.

2 Experimental Program

The experimental investigation consisted of designing, casting and testing of RC beam specimens using a normal grade of concrete mixture. The beams were designed according to ACI 318-14 to ensure failure in shear. Nine RC beams were prepared considering the shear span-to-depth ratio (a/d) and strengthening configuration as two variable parameters. The details of the nine beam specimens are illustrated in Table 1. As can be noted from this table, the beams were retrofitted by applying a 30 mm thick layer of UHPC over the sandblasted faces of the RC beams. UHPC jacketing was done in two different configurations: (i) on two longitudinal vertical faces of the beams and (ii) on two longitudinal vertical faces as well as on the bottom face. In addition, specimens were prepared and tested to evaluate the mechanical properties of concrete mixtures used. Bond testing was carried out to evaluate the bond strength between normal concrete substrate and UHPC.

2.1 Materials Properties

2.1.1 Normal Concrete and Steel Reinforcement for Casting the RC Beams

A normal high-grade concrete mixture was obtained from a local precast concrete factory. Cylindrical specimens (75 mm diameter and 150 mm height) were cast to determine the compressive strength, tensile strength and the modulus of elasticity of the mixture. The Compressive strength and split tensile strength tests were conducted in accordance with ASTM C39 (ASTM International 2017) and ASTM C496 (ASTM International 2004), respectively. The average values of compressive strength, and modulus of elasticity of normal concrete are presented in Table 2 along with the minimum, maximum, and standard deviation values. The 8 mm diameter steel rebars used as shear reinforcement were tested under direct tension and the mechanical properties recorded are listed in Table 3. Figure 1 shows the stress–strain behavior of normal concrete and the shear reinforcement.

2.1.2 UHPC for Strengthening the RC Beams

A typical mixture of UHPC developed by Ahmad et al. (2015) was used for strengthening the prepared RC beams. The mixture proportions of the UHPC, as

Table 1 Details of the beam specimens.

Group	Beam ID	Beam description	Dimensions $b \times h \times L$ (mm)	a/d ratio	Shear span (mm)
First	CT-1.0	Control beam	140 × 230 × 1120	1.0	200
	SB-2SJ-1.0[a]	Beam strengthened by two longitudinal vertical faces	200 × 230 × 1120	1.0	200
	SB-3SJ-1.0	Beam strengthened by jacketing two longitudinal vertical faces and the bottom face	200 × 260 × 1120	1.0	200
Second	CT-1.5	Control beam	140 × 230 × 1120	1.5	280
	SB-2SJ-1.5	Beam strengthened by two longitudinal vertical faces	200 × 230 × 1120	1.5	280
	SB-3SJ-1.5	Beam strengthened by jacketing two longitudinal vertical faces and the bottom face	200 × 260 × 1120	1.5	280
Third	CT-2.0	Control beam	140 × 230 × 1120	2.0	384
	SB-2SJ-2.0	Beam strengthened by two longitudinal vertical faces	200 × 230 × 1120	2.0	384
	SB-3SJ-2.0	Beam strengthened by jacketing two longitudinal vertical faces and the bottom face	200 × 260 × 1120	2.0	384

[a] Beam strengthened by preparing the surfaces using sandblasting technique (*SB*) and applying UHPC to obtain two-side layers (*2SJ*), tested maintaining a shear-span to depth ratio (a/d) of 1.0.

Table 2 Mechanical properties of normal high grade concrete.

Property	Min. value	Max. value	Average value	Standard deviation
Compressive Strength (MPa)	59	71	65	4.6
Modulus of elasticity (GPa)	26	34	31	2.9

Table 3 Mechanical properties of shear reinforcement.

Material	Property	Average value
Steel rebar used as stirrups	Yield strength (MPa)	610
	Modulus of elasticity (GPa)	200.6
	Ultimate strength (MPa)	710.1

adopted from Ahmad et al. (2015) are presented in Table 4. Two types of steel fibers of a tensile strength 2500 MPa (straight and hooked) were added in a mass ratio of 1:1 for increasing the interlocking between fibers and therefore increasing the crack bridging. Straight fibers had a diameter of 0.1 mm and a length of 12.5 mm and hooked fibers had 0.2 mm in diameter with a length of 25 mm.

The compressive strength of UHPC was measured by testing a total of 15 cubical specimens of 50 mm size in accordance with ASTM C109 (ASTM International 2016) after moist-curing for 28 days. For modulus of elasticity test, eight cylindrical specimens of size 75 × 150 mm were prepared and moist-cured for 28 days. Stress–strain data were recorded by applying the uniaxial compressive load, as shown in Fig. 2. The stress versus strain data was plotted, some of them are shown in Fig. 3, for determining the modulus of elasticity. Using the linear part of stress–strain curve, the modulus of elasticity was calculated using the ASTM C469 (ASTM International 2014). The direct tensile strength of UHPC was measured using six dogbone-shape specimens having a square cross-section of 40 mm size. The test setup, as shown in Fig. 2, consisted of the UTM machine, load cell, prototype frame, data logger, LVDT, and two extensometers of 50 mm gauge length. The tensile load was applied at a rate of 0.5 mm/min in order to monitor the first crack and capture the strain resulting in the specimen. The stress–strain curve resulting from the direct tension test on dogbone specimens for determining tensile strength of UHPC is shown in Fig. 3. The compressive strength, modulus of elasticity and direct tensile strength of the UHPC mixture are presented in Table 5.

2.1.3 Evaluation of Bond Strength Between Normal Concrete and UHPC

The information regarding strength of bond between a substrate normal concrete-to-a normal overlay concrete is reported in the literature (Momayez et al. 2005), (Julio et al. 2004). Besides the degree of roughness of the substrate, the bond strength is governed by the mechanical characteristic of substrate and overlay concretes, specially, the tensile strength that controls crack development at the interface (Bakhsh 2010). For assessment of the bond quality of composite materials, i.e., normal concrete (NC) and UHPC, splitting tensile strength and slant shear strength tests were conducted using cylindrical specimens. For preparing a composite cylindrical specimen, first a cylindrical specimen was cast using the NC. Then, for splitting tensile strength

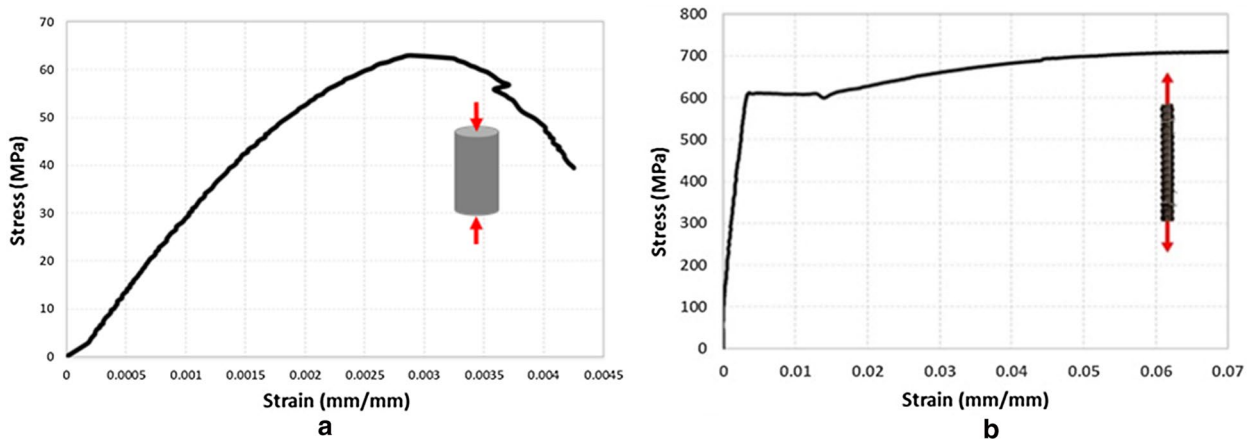

Fig. 1 Stress-strain behavior **a** normal concrete, **b** shear reinforcement.

Table 4 Mixture proportions of UHPC for 1 m^3 (Ahmad et al. 2015).

Ingredients	Cement	Micro-silica	Fine quartz sand	Water	Superplasticizer	Steel fibers
Quantity (kg)	900	220	1005	163	40	157

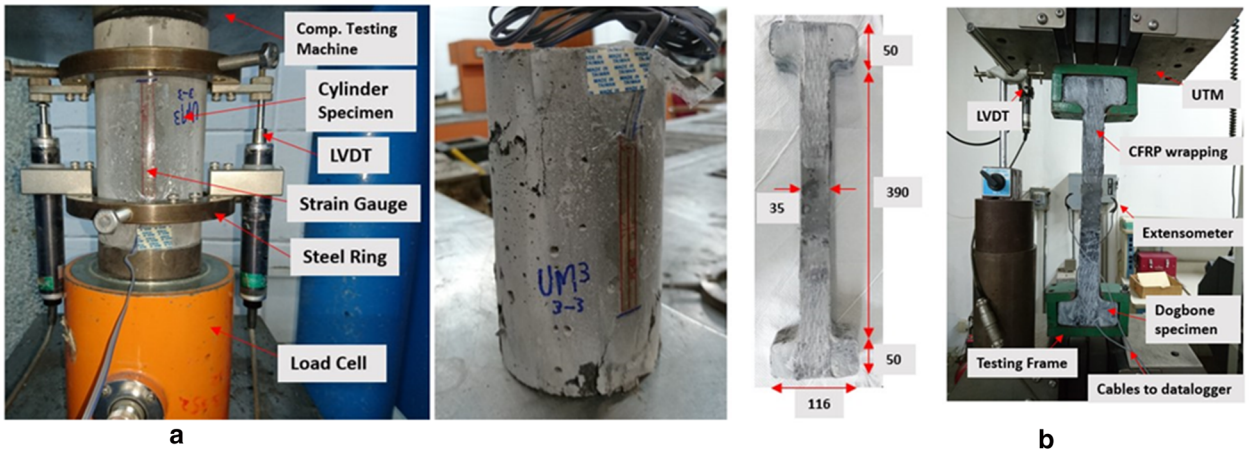

Fig. 2 Test setup **a** uniaxial compressive test on cylindrical specimen of UHPC, **b** uniaxial direct tensile test of UHPC dogbone specimen (all dimensions in mm).

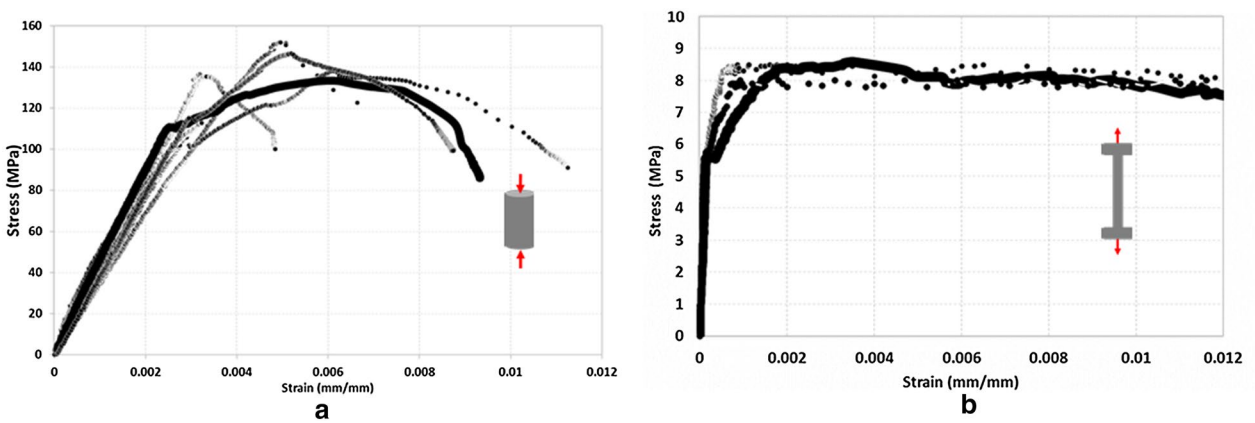

Fig. 3 Typical stress–strain behavior of UHPC, **a** in compression **b** in tension.

Table 5 Mechanical properties of UHPC.

Property	Average value
Cubical compressive strength (MPa)	151.4
Direct tensile strength (MPa)	8.7
Modulus of elasticity (GPa)	41.0

test, the cylinder was halved longitudinally using a concrete cutting machine. The halved cylinder of NC was sandblasted for a depth of 2 mm and then kept in a cylindrical mold. UHPC was then poured into the mold to obtain a composite cylindrical specimen comprising of NC and UHPC. Same procedure was used to prepare the composite cylindrical specimen with a slant interface (30° plane) between NC and UHPC for slant-shear strength test.

In splitting tensile strength test, the composite cylindrical specimen was placed horizontally in the testing machine and the load was applied along specimen's length in accordance to ASTM C496 (ASTM International 2004), as shown in Fig. 4. The load was applied until the tensile failure occurred. The splitting tensile strength of composite specimen was calculated using the equation provided by ASTM C496 (ASTM International 2004). Slant-shear strength test was conducted according to ASTM C882 (ASTM International 2013), as shown in Fig. 4. Bond strength was calculated by dividing the failure load by elliptical bonding area between the NC and UHPC.

For both tests, the failure took place at the interface and partially at the substrate as shown in Fig. 4. The bond strengths measured using both tests are presented in Table 6 and compared to the range recommended by ACI 546.3R-14 (2014). The proposed ACI range provides

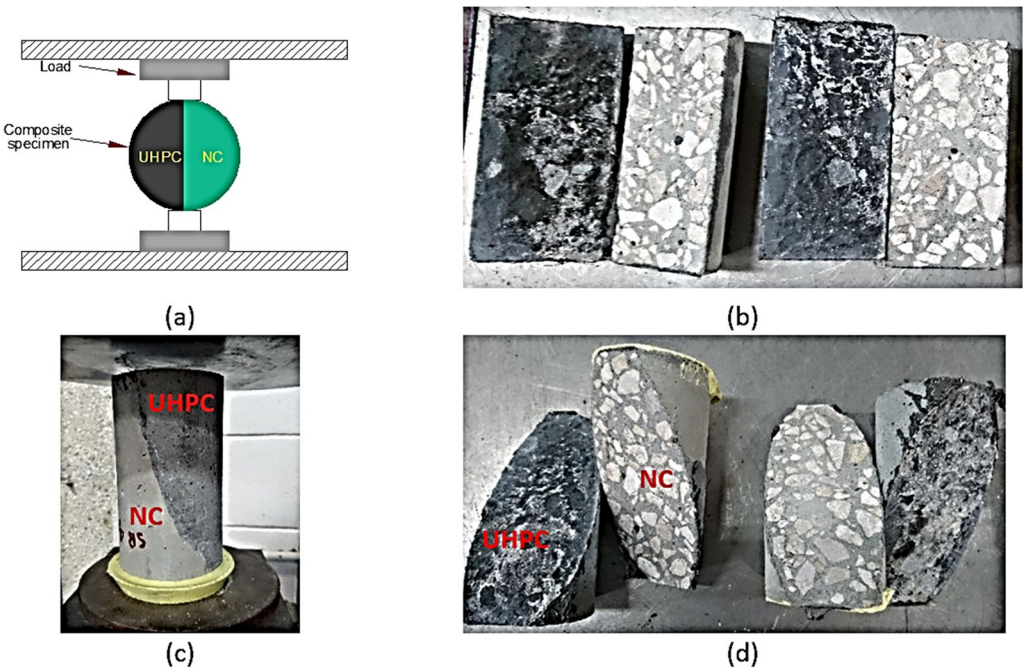

Fig. 4 **a** Splitting tensile test setup, **b** failure mode of splitting tensile test, **c** slant-shear strength test setup, **d** failure mode of slant-shear strength test.

Table 6 Average bond strengths.

Using slant-shear test	Using splitting tensile test
22.91 MPa (the range recommended by ACI 546-14: 14–21 MPa)	3.41 MPa (the range recommended by ACI 546-14: 1.7–2.1 MPa)

the minimum acceptable values for bond strength and it is useful only for evaluation of the bond requirements for quality compliance purpose and not for the design purpose. As can be seen from Table 6, the results of both tests were more than the recommended ranges, indicating adequate bonding between NC and UHPC.

2.2 Casting and Strengthening of the RC Beam Specimens

In all the nine RC beams, two steel rebars having 20 mm diameter were placed in tension zone and two rebars of 12 mm diameter were kept in the compression zone. The shear reinforcement was provided in the form of two-legged stirrups of 8 mm diameter at a spacing of 120 mm. As indicated in Table 1, all beams had identical cross-section as 140 mm wide by 230 mm deep (before strengthening) with an overall length of 1120 mm. The reinforcing steel cages were prepared and a 20 mm clear cover was provided at all sides using plastic spacers. The NC was used for casting the RC beams.

Prior to casting of UHPC over the surfaces of the RC beams, the beam surfaces were prepared by applying sandblasting up to a depth of 2 mm to obtain a rough surface, as shown in Fig. 5. The sandblasted RC beams were kept in the mold maintain the gap for casting the UHPC over the intended faces of the RC beams, as shown in Fig. 5. As mentioned earlier, the strengthening was carried out using two configurations: (i) three-sided jacketing and (ii) two-sided layers over the entire length of the beam, as shown in Fig. 5. After casting the UHPC over the surfaces of RC beams, the specimens were immediately covered by wet burlap and plastic sheets for first 24 h. After 24 h of casting, all the strengthened RC beam specimens were demolded and taken out to the curing tank for 28 days curing. Figure 6 shows the details of the control and strengthened RC beam specimens.

2.3 Testing of Beam Specimens

The control and strengthened beam specimens were tested under the four-point loading arrangement, as

Fig. 5 **a** Applying sandblasting, **b** placing sandblasted RC beam in mold, **c** casting UHPC directly on the RC beams.

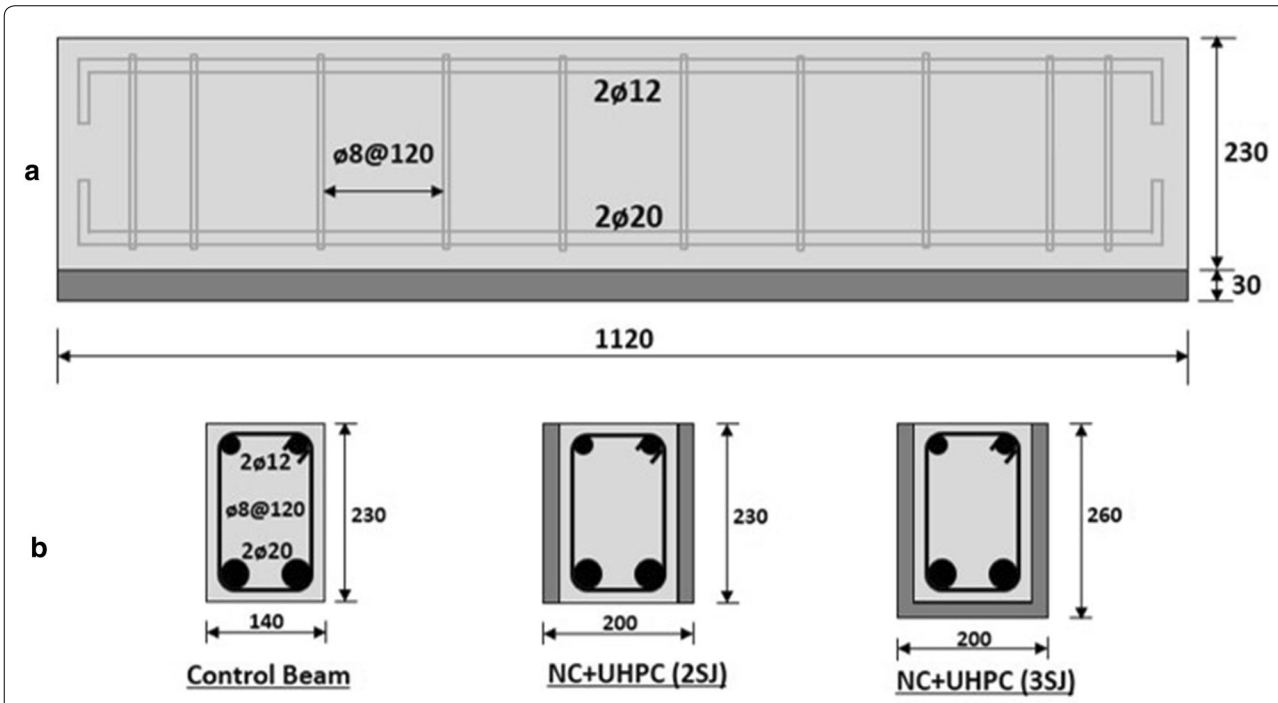

Fig. 6 **a** RC beam details, **b** strengthening configurations (all dimensions in mm).

shown in Fig. 7. The beam specimen was placed in the testing frame, then all the instruments/accessories required for applying the load and recording the deformation were set in their positions. The displacement-control load (at rate of 0.5 mm/min) was applied monotonically until the failure was occurred. The information that were recorded during the beam test included: crack patterns, bond between NC and UHPC, and failure modes. The load versus mid-span deflection data was plotted and such curves were analyzed to understand the behavior of tested beam.

3 Numerical Modelling

In addition to the experimental investigation, a numerical modelling was carried out using finite element method to study the shear behavior of the strengthened beams. The main purpose of the numerical modelling in the present study was to confirm the sufficiency of the experimental data for highlighting the shear behavior that included depiction of load versus deflection plots, failure loads and cracking patterns.

The numerical modeling was developed using the *Abaqus* finite element analysis software. The finite element model consisted of modelling the geometry of elements with their materials and related constraints, such as boundary conditions, applying loads and the contacts

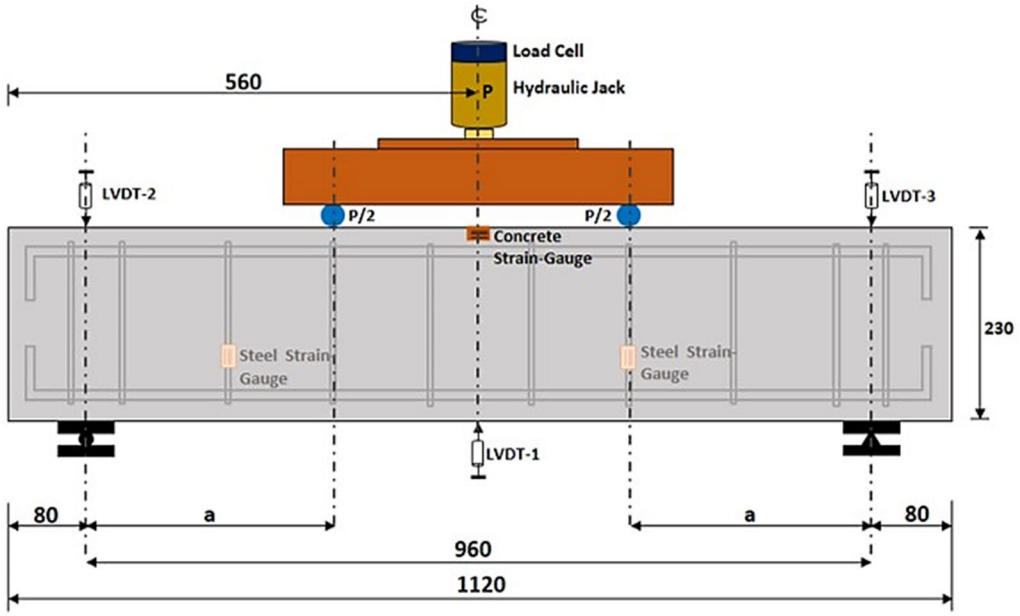

Fig. 7 Schematic representation of beam testing setup (all dimensions in mm).

between the different surfaces. The normal concrete, UHPC, and steel-plates were modeled using the three-dimensional eight-noded brick elements. Whereas, the reinforcement steel (longitudinal and transverse) were modeled with two nodes 3D truss elements. The bond between concrete and reinforcement steel was modeled as an embedded region, whereas the concrete is considered as the host element. The bond between normal concrete and UHPC was considered as perfect-bond because during all experimental tests there was no debonding observed. The steel plates were bonded to the concrete surfaces with tie-bond. The concrete damage plasticity model was used, which is reported to give reliable results (Sümer and Aktaş 2015). Accordingly, by using such model, the complete behavior of full-scale strengthened beams can be achieved without conducting any experimental testing of beam.

3.1 Concrete Damage Plasticity Model

The plasticity theory is commonly used in modelling the quasi-brittle materials such as a concrete. However, the use of plasticity theory is suitable only in compression zones. Several models based on fracture mechanics such as: smeared crack model, fictitious crack model, and crack-band theory are used in tension zones (Lee and Fenves 1998). Therefore, an approach is needed that could consider the non-linear behavior of concrete in a single constitutive model. Lubliner and Oliver (Lubliner et al. 1989) formulated a plastic damage model for concrete based on the plasticity theory.

Concrete damage plasticity (CDP) approach develops the constitutive behavior of concrete by presenting the scalar damage variables for both compressive and tensile response as illustrated in Fig. 8. The damage variables in tension and compression are denoted by d_t and d_c, respectively. The values of d_t and d_c range from zero to one. *Abaqus* user manual assumed zero for undamaged material and one for completely damaged (i.e., loss of stiffness) (Online Documentation Simulia 2016).

The CDP approach describes mainly two failure mechanisms, tensile cracking and compressive crushing of concrete. The yield surface is governed by two hardening variables ε_t^{PL} and ε_c^{PL}, which are associated to the failure mechanisms under tension and compression loading, respectively. The compressive and tensile damage parameters are calculated based on the equations provided by Birtel and Mark (Birtel 2007):

- Compressive damage parameter (d_c):

$$d_c = 1 - \frac{\sigma_c E_c^{-1}}{\varepsilon_c^{pl}(1/b_c - 1) + \sigma_c E_c^{-1}}. \quad (1)$$

- Tensile damage parameter (d_t):

$$d_t = 1 - \frac{\sigma_t E_c^{-1}}{\varepsilon_t^{pl}(1/b_t - 1) + \sigma_t E_c^{-1}}. \quad (2)$$

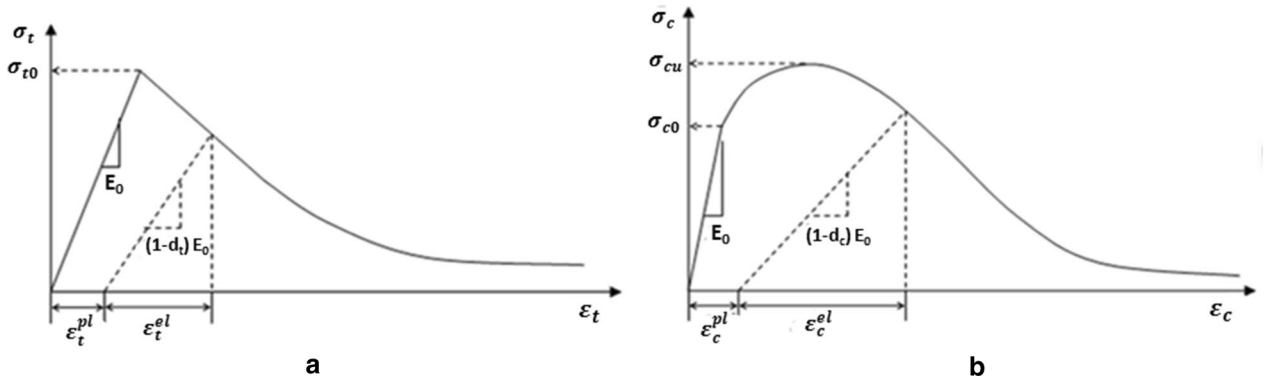

Fig. 8 Damage variables: **a** in tension, **b** in compression (Online Documentation Simulia 2016).

where d_c and d_t are compressive and tensile damage parameters, σ_c and σ_t are compressive and tensile stresses of concrete, E_c is the modulus of elasticity of concrete, ε_c^{pl} and ε_t^{pl} are plastic strains corresponding to compressive and tensile strengths of concrete. b_c and b_t are constant parameters, $0 < b_{c,t} \leq 1$.

3.2 FE Modeling Considerations

The materials (normal concrete, UHPC and steel reinforcement) were modeled using the data generated through the experimental program. The nonlinear behavior in tension as well as in compression of both the normal concrete and UHPC, as shown in Fig. 9, were used.

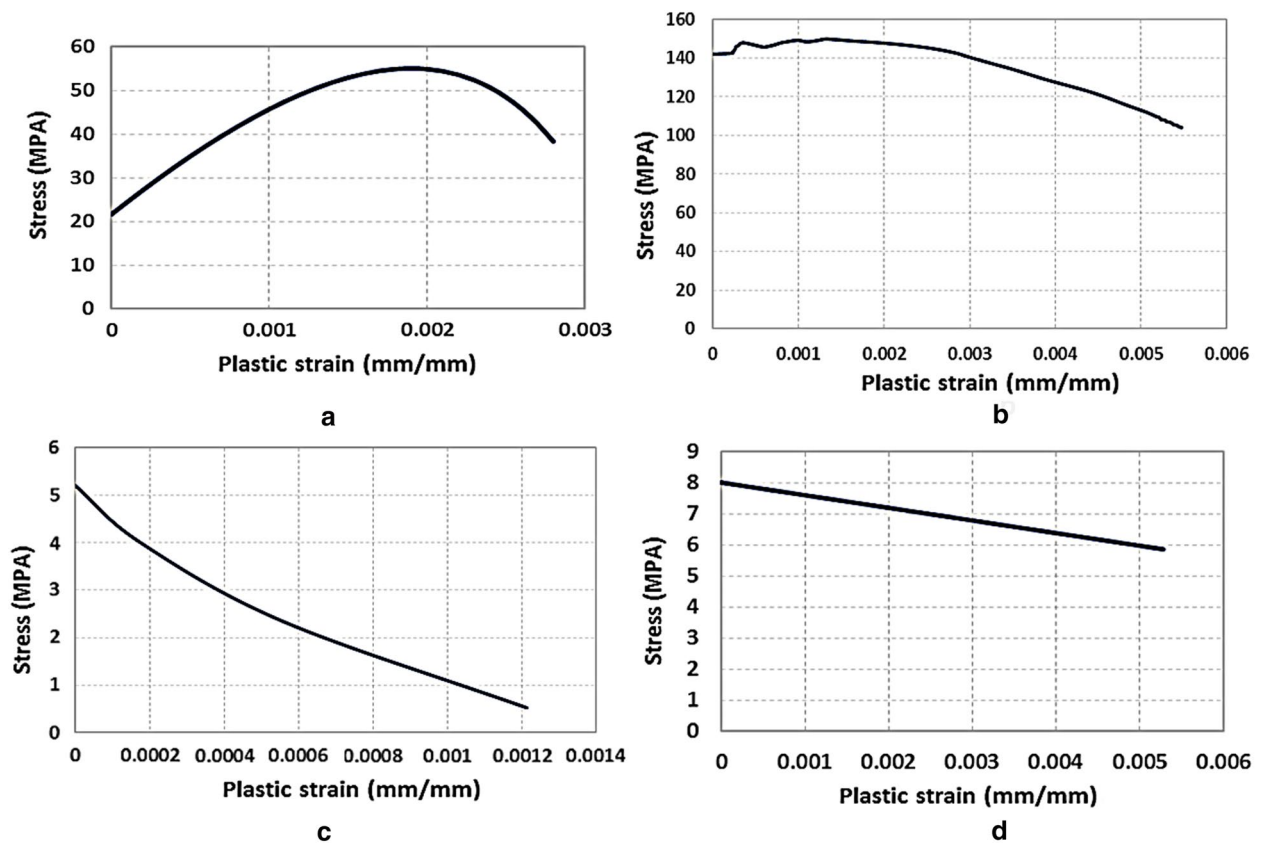

Fig. 9 Nonlinear behaviour of materials: **a** normal concrete in compression **b** normal concrete in tension **c** UHPC in compression **d** UHPC in tension.

The bonding between different surfaces was modelled using the available options in *Abaqus* library. The bond between concrete and reinforcement steel was taken as embedded region, where the concrete is the host element. The adhesion between normal concrete and UHPC was considered as perfect-bond because during all experimental tests, debonding was not observed.

In *Abaqus*, the most dependable approach of applying the load is the explicit dynamic method. This method is reported to be successful for two main reasons: first, it gives reliable results with less problems of convergence, second, it is the most suitable for materials like concrete to capture the concrete cracks and overall failure behavior (Mercan 2011). Furthermore, in explicit dynamic analysis, the inertial effects can be minimized by either reducing the loading rate or increasing the mass density of concrete in order to approach the static solution. Thus, in *Abaqus*, the time increments are automatically calculated and the loading rate is set as one second.

All experimental results, including failure load, crack pattern, failure mode and load–deflection curves were compared with those obtained through the FE modelling. This comparison showed that the FE model is able to capture most of the failure modes with good accuracy.

4 Results and Discussion

4.1 Experimental Data

4.1.1 Beam Specimens with a/d = 1.0

In this category, three beams were tested, one was control beam and the remaining two beams were strengthened using UHPC with two different configurations, as mentioned in Table 1. All three beams in this group were tested keeping a shear span-to-depth ratio (*a*/*d*) of 1.0 by maintaining the shear span, *a*, at 200 mm.

For control beam specimen (*CT-1.0*), the hairline vertical cracks initiated near the point of maximum moment. As load increased, the diagonal cracks started appearing and these diagonal cracks propagated in the shear region spanning over 200 mm (i.e., within the shear span). Then it failed suddenly in pure shear at a load of 383 kN, as shown in Fig. 10, which represents the crack patterns at the failure stage when the collapse load was recorded. The load–deflection curve, as shown in Fig. 11, shows a descending part of the curve, which also indicates a sudden failure after reaching the ultimate load with corresponding displacement of 2.17 mm.

In case of beam specimen, strengthened by UHPC applied from two opposite sides (*SB-2SJ-1.0*), the flexural

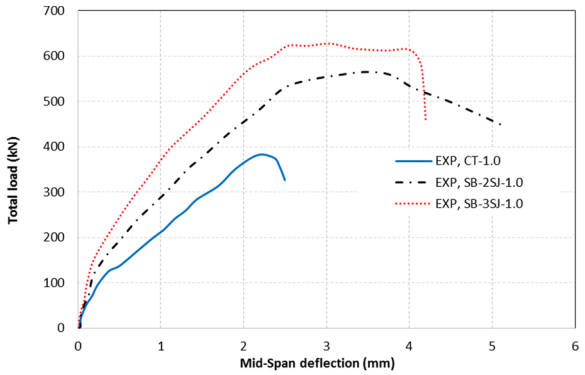

Fig. 11 Load–deflection curves of all beams with *a*/*d* = 1.0.

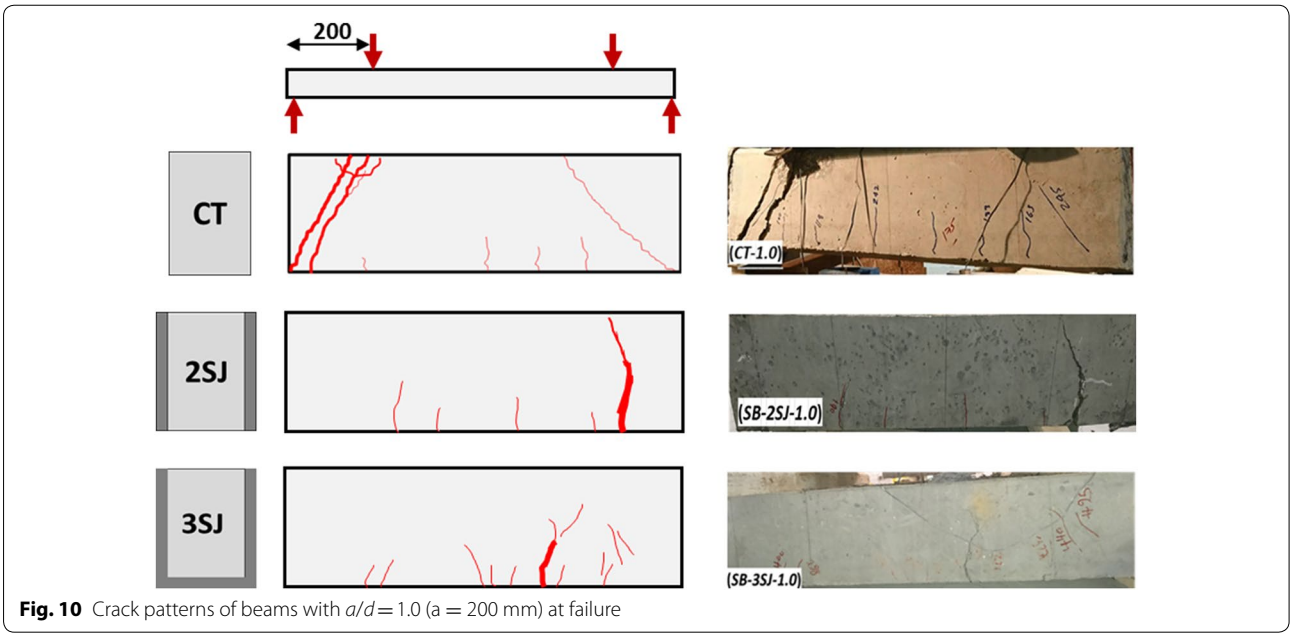

Fig. 10 Crack patterns of beams with *a*/*d* = 1.0 (a = 200 mm) at failure

cracks (vertical cracks) were initiated at the mid span of beam followed by the secondary inclined cracks, as shown in Fig. 10. The beam failed in combined shear and flexure (flexure-shear mode) at an ultimate load of 567 kN with corresponding midpoint displacement of 3.47 mm, as can be observed from Fig. 11. The UHPC strips acted as vertical reinforcement to carry more shear load in addition to the contribution of the shear stirrups and the concrete towards the total shear capacity. This enhanced shear capacity of the beam resulted into the increase in the failure load and shifting of the failure mode from pure shear to flexure-shear mode. The failure load of the beam *SB-2SJ-1.0* was found to be 48% more than that of the control beam. In addition, changing the failure mode from pure shear, which is considered a sudden and catastrophic, to flexural-shear failure is an added advantage of such strengthening technique.

The third beam in this group was strengthened from three sides (*SB-3SJ-1.0*). This beam failed in flexure within the constant-moment region where fewer vertical cracks started and propagated, as shown in Fig. 10. The ultimate load was found to be 628 kN (63% greater than the control beam) and corresponding midspan displacement of 3.10 mm. The UHPC strengthening from three sides completely changed the failure from pure shear to flexure mode with further enhancement in the failure load. This can be attributed to the joint effect of UHPC strips on sides and at bottom of the beam. The bottom UHPC strip together with the side strips slightly enhanced the shear. The enhancement of flexural capacity due to the bottom strip resulted into an increase in the collapse load with a ductile mode of failure, as can be observed from the crack patterns and load–deflection curves shown in Figs. 10 and 11, respectively.

Although, the beams failed at relatively high load, no de-bonding occurred between the substrate and overlay indicating an excellent bonding between NC and UHPC.

4.1.2 Beam specimens with a/d = 1.5

In this group of beams, the shear span, a, was kept as 280 mm to maintain a shear-span to depth ratio of 1.5 ($a/d = 1.5$). Three beams were tested including control beam and two strengthened beams. It can be seen from Fig. 12 that the reference beam (*CT-1.5*) had diagonal cracks within the shear span and failure took place suddenly in the crushing zone near the loading point, which is characterized as shear compression failure, similar to the previous case with $a/d = 1$, as can be observed from Fig. 13. However, the ultimate load was 286 kN and corresponding midpoint displacement of 4.40 mm, which is less than that for beam (*CT-1.0*) with $a/d = 1.0$. This is because of the fact that at a higher a/d ratio, the effect of the arch action and dowel action is less which results in a lower shear capacity.

The strengthened beam from two sides (*SB-2SJ-1.5*), firstly forming a vertical crack in the shear zone, then it bent over to form an inclined crack and ultimately a small spalling of concrete was noted near the support at the failure stage, as can be seen from Fig. 12. The appearance of a mixed vertical-inclined crack may be attributed to the fact that, in spite of strengthening, the shear capacity of the beam remained lower than its flexural capacity and the shear failure dominated over the flexural failure. This combined mode of failure of the beam *SB-2SJ-1.5*

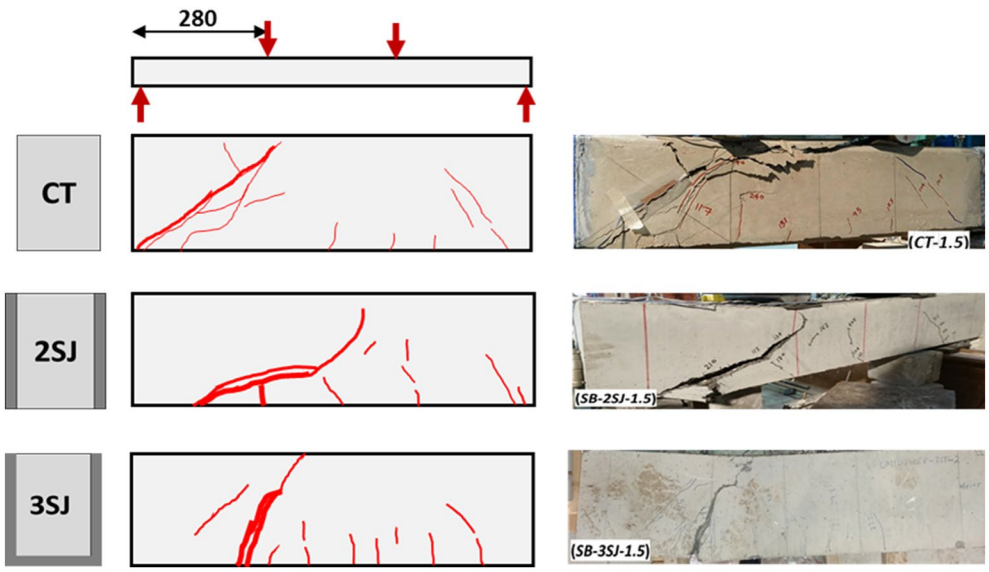

Fig. 12 Crack patterns of beams with $a/d = 1.5$ (a = 280 mm) at failure.

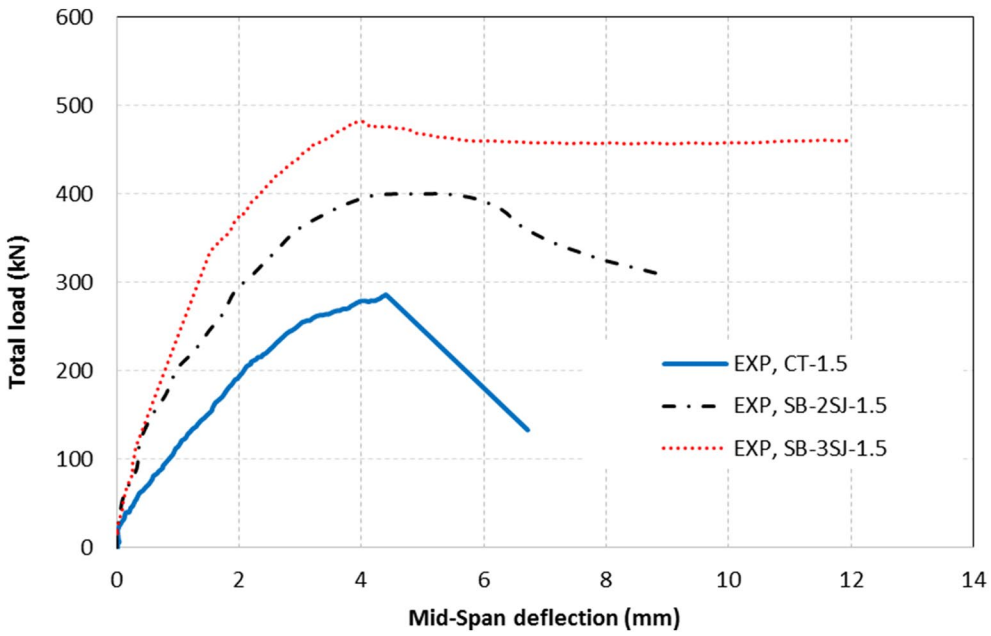

Fig. 13 Load–deflection curves of all beams with $a/d = 1.5$.

can also be observed from the load–deflection curve as shown in Fig. 13, which shows more ductile behavior as compared to the control beam specimen. The failure is similar to the anchorage problem, which is due to insufficient development length of the UHPC jacket beyond the point of support. The failure load was found to be 402 kN and corresponding midpoint displacement of 5.20 mm and with an increase in load carrying capacity by 46% as compared to the control beam (*CT-1.5*).

It can be observed from the crack pattern as shown in Fig. 12, at the failure stage, the vertical cracks appeared and propagated indicating a flexural failure in case of the beam strengthened from three sides (*SB-3SJ-1.5*). The beams failed in pure flexure at ultimate loads of 482 kN and corresponding midpoint displacement of 4.10 mm and with an increase in the load-bearing capacity by 69% as compared to the control specimen. More ductile and stiff behavior of the beam *SB-3SJ-1.5* can be observed in Fig. 13, where the prolonged portion of the peak load–deflection curve can be seen in case the beam *SB-3SJ-1.5*. Moreover, the bonding between the substrate and UHPC layers was intact at the failure, which indicated the UHPC develops the full shear strength until the flexural reinforcement yielded.

4.1.3 Beam specimens with a/d = 2.0

The control and strengthened beam specimens were tested keeping the a/d ratio as 2.0 by maintaining a shear span of 384 mm. Similar to the previous cases, the control beam with a/d ratio as 2.0 (*CT-2.0*) also displayed the shear compression failure by forming diagonal cracks joining the points of load application and support, as can be seen from Fig. 14, which represents the crack patterns at the failure stage. This beam failed at an ultimate load of 276 kN with a little softening behavior (Fig. 15). The midpoint displacement corresponding to the failure load was 7.0 mm. The beam strengthened from two sides (*SB-2SJ-2.0*) failed in flexure-shear mode, as can be observed from Fig. 14. It had an ultimate load capacity of 346 kN and corresponding midpoint displacement of 7.5 mm, a value 25% higher than that of the control beam. The beam strengthened from three sides (*SB-3SJ-2.0*) failed in flexure by forming a macro vertical crack located in the maximum bending moment zone (between the two-point loads), as shown in Fig. 14. It possessed an ultimate load carrying capacity of 353 kN, a value 28% higher than that of the control beam, very similar to the case of two-side strengthened beam, indicating that there is no significant effect of the strengthening configuration at a higher a/d ratio. Further, both strengthened beams showed an excellent ductile behavior. However, the three-sided strengthened beam had a lower deflection at ultimate load and had a better stiff behavior

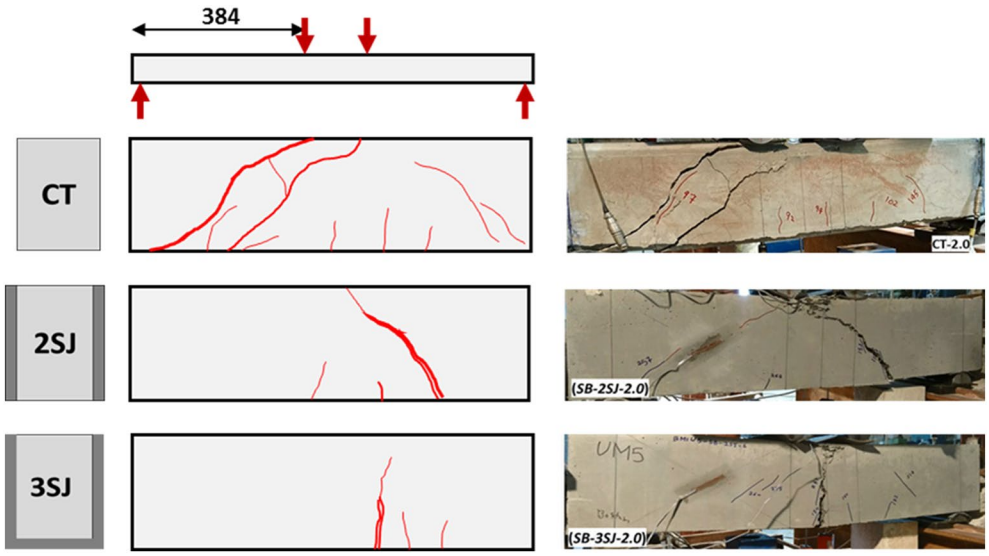

Fig. 14 Crack patterns of beams with $a/d = 2.0$ (a = 384 mm) at failure

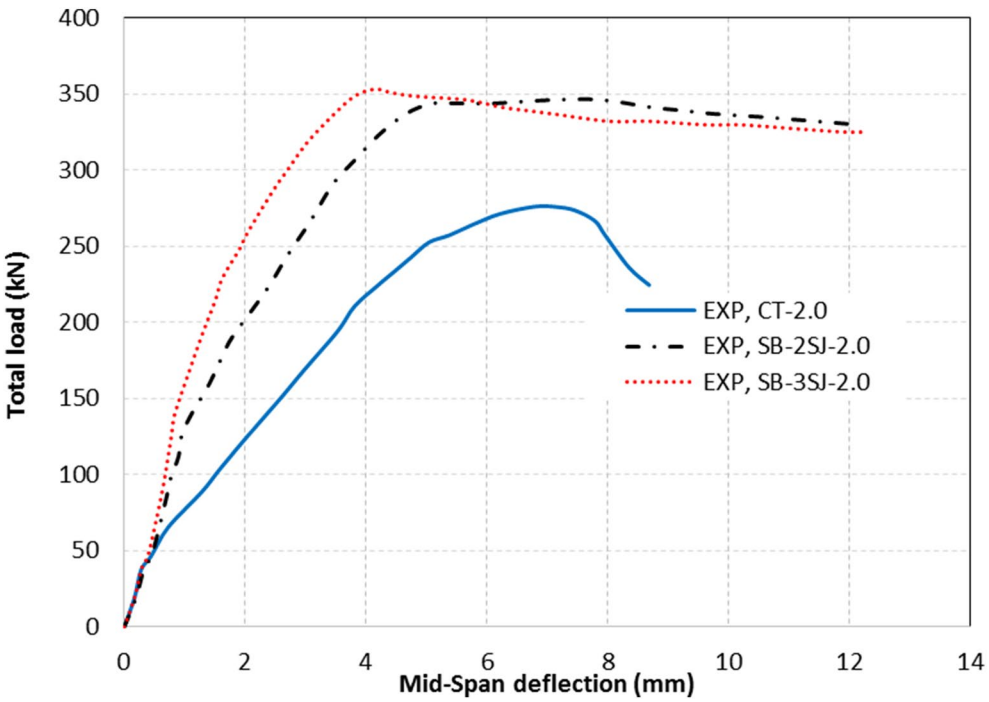

Fig. 15 Load–deflection curves of all beams with $a/d = 2.0$.

than the two-sided strengthened beam, as can be seen from Fig. 15. Generally, because of strengthening using UHPC, the shear capacity and the ductile behavior of the beams got enhanced. However, the significant effect of strengthening configurations (two-sided or three-sided jacketing) on the contributions of UHPC strengthening was noticed.

Table 7 Summary of the results of tested beams.

Beam ID	*a*/*d* ratio	Ultimate load (kN)	Deflection at ultimate (mm)	Maximum deflection (mm)	Comparison of failure load (%)	Failure mode
CT-1.0	1.0	383	2.17	2.49	0 (control)	Shear
SB-2SJ-1.0	1.0	567	3.47	5.11	48	Flexure–shear
SB-3SJ-1.0	1.0	628	3.10	4.19	63	Flexural
CT-1.5	1.5	286	4.40	6.72	0 (control)	Shear
SB-2SJ-1.5	1.5	402	5.20	8.96	41	Flexure–shear
SB-3SJ-1.5	1.5	482	4.10	11.98	69	Flexural
CT-2.0	2.0	276	7.00	8.68	0 (control)	Shear
SB-2SJ-2.0	2.0	346	7.50	12.15	25	Flexure–shear
SB-3SJ-2.0	2.0	353	4.14	12.26	28	Flexural

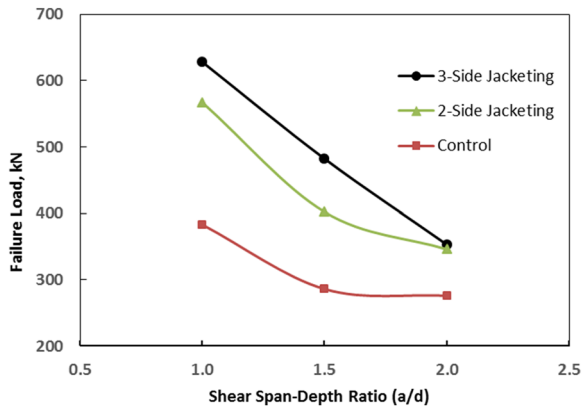

Fig. 16 Effect of *a*/*d* ratio and strengthening configuration on load-carrying capacity.

4.1.4 Summary of the Beam Test Results

Table 7 presents a summary of the results of all nine tested beam specimens. As expected, all the control beams failed suddenly in shear by forming a diagonal crack. It can be concluded that UHPC strengthening can significantly increase the serviceability, ductile behavior and ultimate shear strength of concrete beams. In case of two-sided strengthened beams, the failed mode was shifted from shear to flexure-shear and the failure in three-sided strengthened beams was shifted to flexural mode. There is a substantial increase in the load carrying capacity of the strengthened beams. However, the positive effect of the strengthening is more up to the *a*/*d* ratio of 1.5 than the *a*/*d* ratio of 2.0. Furthermore, the increase in load-carrying capacity due to addition of bottom layer is up to the *a*/*d* ratio of 1.5, the load-carrying capacity of two-sided as well as three-sided strengthened beams was almost same at *a*/*d* ratio of 2.0. The effect of *a*/*d* ratio and strengthening configuration on load-carrying capacity is shown in Fig. 16. It is observed that as the *a*/*d* ratio increased, the shear capacity of the beams decreased due to the ineffectiveness of the contributions of shear load transfer mechanisms. For the control beam with $a/d = 1.0$, the behavior is similar to the deep beams and the failure is generally governed either by shear-compression or by tension failures. However, for retrofitted beams with same ratio ($a/d = 1.0$), the behavior becomes more ductile and the cracks tend to be vertical as a case of a long conventional beam with high *a*/*d* ratio. This may be attributed to the ability of UHPC jacketing to redistribute the shear stress. For other *a*/*d* ratios ($a/d = 1.5$ and 2.0), a similar trend was observed, as shown in Fig. 16, with much lower in the shear capacity, and the UHPC jacketing recovered these reductions in shear strength.

4.2 FEM Results Compared with Experimental Data

4.2.1 Beams Specimens with a/d = 1.0

The FEM results (load–deflection plots and cracking patterns) obtained for the two beams with shear span-to-depth ratio of 1.0 (*CT-1.0 and SB-2SJ-1.0*) are shown in Figs. 17, 18, 19 along with the experimental results for comparison purpose. The control beam (*CT-1.0*) failed in diagonal tension crack (i.e., in shear failure) at a load of 373 kN, as shown in Fig. 17. The retrofitted beam (*SB-2SJ-1.0*), which was strengthened by UHPC on two-sides, was broken due to flexure-shear crack at a failure load of 546 kN, as shown in Fig. 18. For beam strengthened on three sides (*SB-3SJ-1.0*) failed in pure flexure failure at ultimate load of 611 kN. It can be observed from Figs. 17, 18, 19, the FEM results of this group of beams are in good agreement with the corresponding experimental test results. For control beam (*CT-1.0*), the experimental value of failure load was 383 kN against the failure load 373 kN predicted by FEM with a difference of 3% only. The crack patterns for the control beam (*CT-1.0*) obtained from FEM showed a clear shear compression failure at constant shear region, as shown in Fig. 17. FEM captured the failure pattern of retrofitted beam (*B-2SJ-1.0*), as shown in Fig. 18. The crack pattern showed

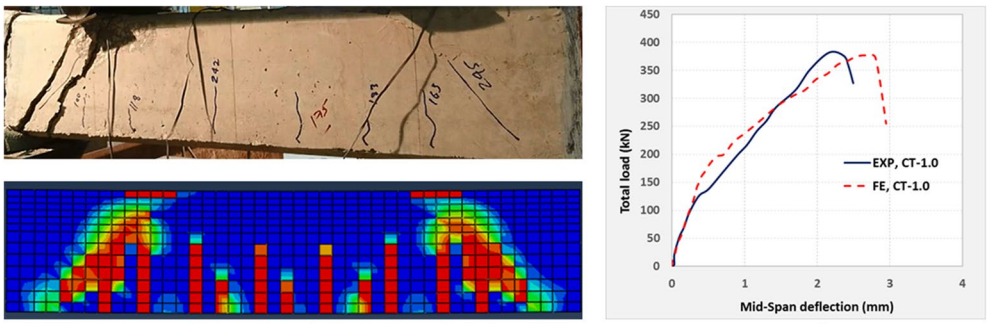

Fig. 17 Control beam (CT-1.0): **a** failure mode of experimental and FE, **b** load–deflection response.

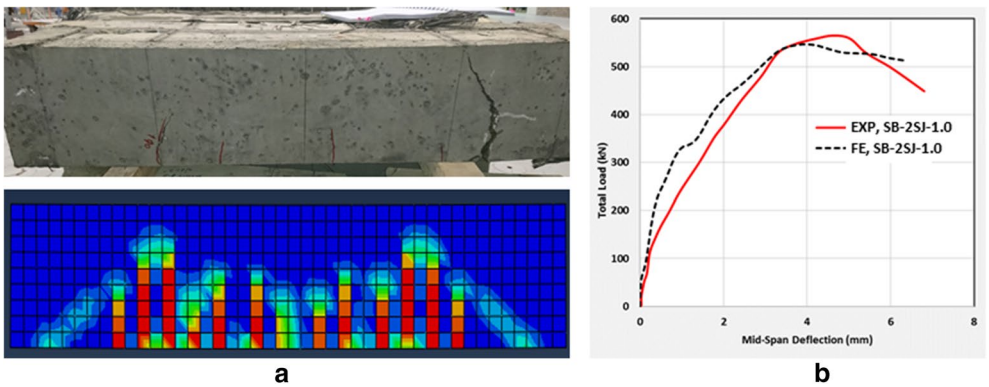

Fig. 18 Retrofitted I beam (SB-2SJ-1.0): **a** failure mode, **b** load–deflection response.

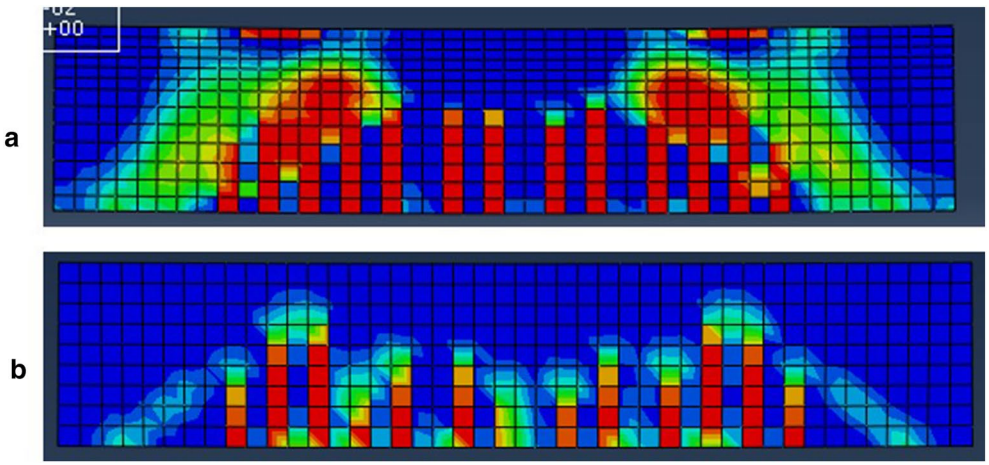

Fig. 19 Retrofitted beam (SB-2SJ-1.0): **a** interfacial surface of NC—shear failure, **b** flexural failure at retrofitted beam.

a flexure shear failure at a maximum load of 546 kN, whereas the test failure load was 567 kN (with a deviation of only 3.8%). Figure 18 shows the load–deflection curve where a slight reduction in the slope of experimental curve can be observed after elastic region, this is probably because of the effect of orientation of steel fibers, which affect the experimental results. Moreover, in *Abaqus*, the damage of interfacial side of normal concrete beam

(original beam) can be observed. It can be seen clearly from Fig. 19 that the failure mode is shifted from diagonal shear crack to a combination of flexure and shear cracks. This indicates that the UHPC strips attached for strengthening take the load once the inclined crack is initiated and the internal forces are redistributed, this action is in the similar way to the role of steel stirrups.

4.2.2 Beams Specimens with a/d = 1.5

The three beams having a/d ratio of 1.5 were modeled in this group that included *CT-1.5, SB-2SJ-1.5*, and *SB-3SJ-1.5*. The failure load for the control beam (*CT-1.5*) using FEM was determined as 294 kN and the crack pattern obtained was in the form of the tension crack (shear-failure), as shown in Fig. 20. The failure loads and cracking patterns for the remaining two beams (SB-2SJ-1.5 and SB-3SJ-1.5) as obtained from the FEM are shown in Figs. 21 and 22, respectively. It can be seen that the failure loads for the beams *SB-2SJ-1.5* and *SB-3SJ-1.5* were 407 kN and 486 kN, respectively. The cracking patterns for the beams *SB-2SJ-1.5* and *SB-3SJ-1.5*, as established through FEM and shown in Figs. 21 and 22, indicate flexure-shear failure and pure flexural failure, respectively. The load–deflection curves of FEM were in good agreement with the experimental results. The shear failure was dominant in control beam (*CT-1.5*) with diagonal crack. The FEM overestimated the peak load by 3% as compared to corresponding experimental value of 286 kN. In addition, a crushing in concrete was observed in experimental test at loading location, which is well predicted by FEM as shown in Fig. 20. The retrofitted beams (*SB-2SJ-1.5* and *SB-3SJ-1.5*) failures loads were in agreement with experimental results with a difference of only 1%, as shown in Figs. 21 and 22.

4.2.3 Beams Specimens with a/d = 2.0

The results of FEM of the last group of three beams having a/d ratio of 2.0 are discussed in this section. The FEM results of the control beam (*CT-2.0*) indicate the failure at a load of 270 kN with dominancy of shear

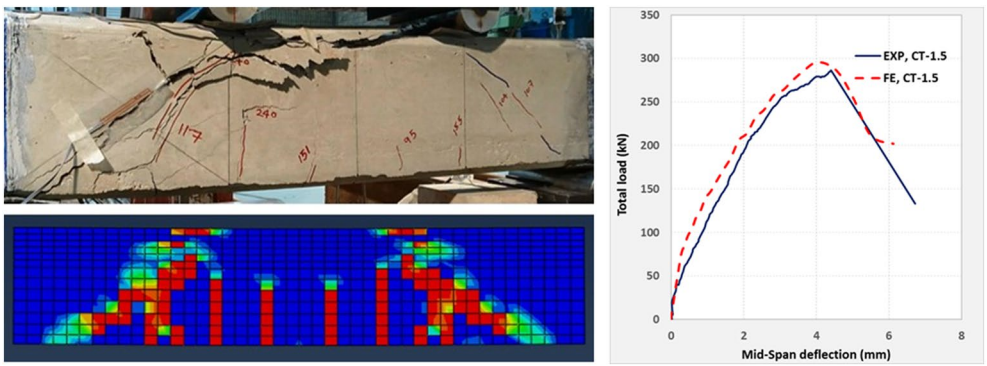

Fig. 20 Control beam (CT-1.5): **a** failure mode, **b** load–deflection response.

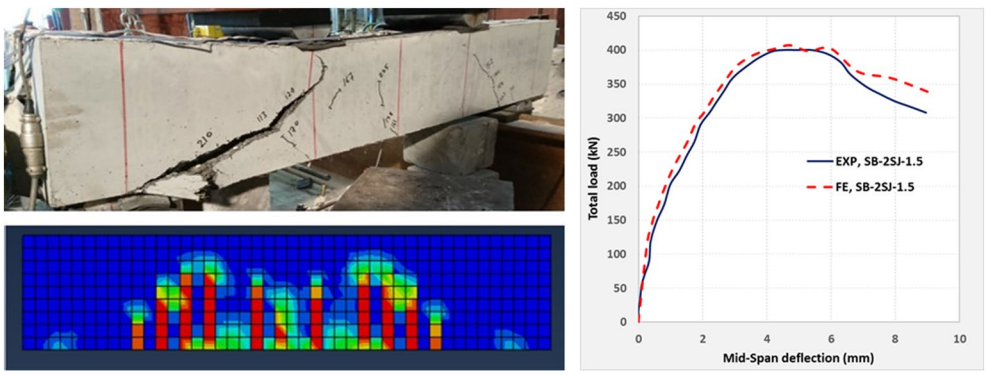

Fig. 21 Retrofitted beam (SB-2SJ-1.5): **a** failure mode, **b** load–deflection response.

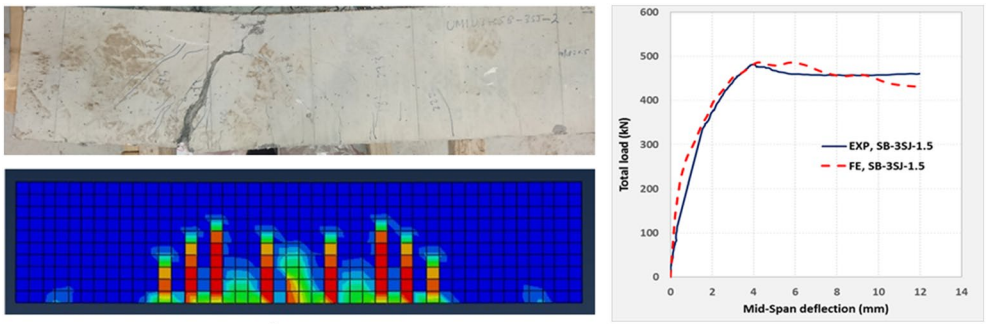

Fig. 22 Retrofitted beam (SB-3SJ-1.5): **a** failure mode, **b** load–deflection response.

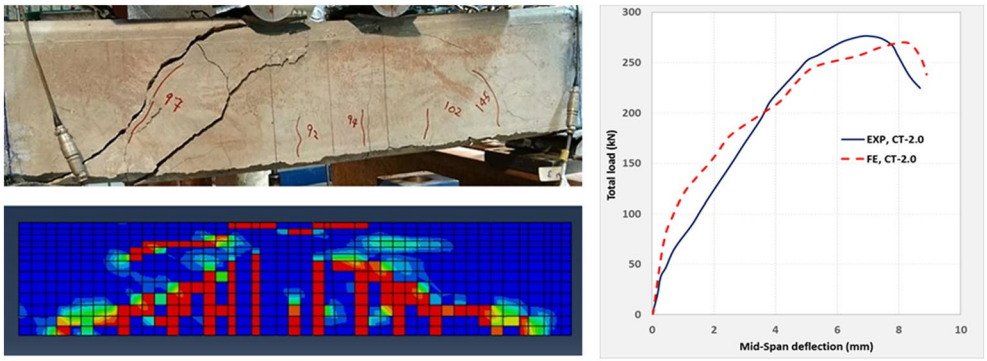

Fig. 23 Control beam (CT-2.0): **a** failure mode, **b** load–deflection response.

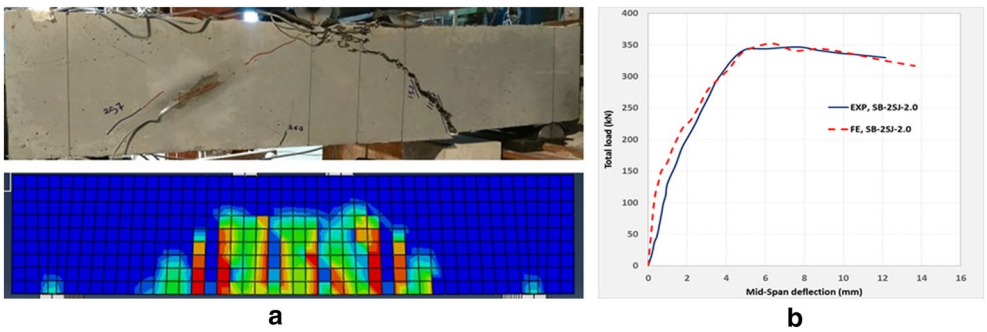

Fig. 24 Retrofitted beam (SB-2SJ-2.0): **a** failure mode, **b** load–deflection response.

failure, as shown in Fig. 23. Similar to the former cases, the strengthened beams (*SB-2SJ-2.0* and *SB-3SJ-2.0*) failed in flexure-shear and pure flexural failures, as can be observed from Figs. 24 and 25, respectively. The failure loads for *SB-2SJ-2.0* and *SB-3SJ-2.0* as predicted by the FEM are 352 kN and 344 kN, respectively, and the experimental data matched very well with the FEM data. It can be observed from Figs. 23, 24, 25 that the failure modes of the beams in this group (*CT-2.0*, *SB-2SJ-2.0*, and *SB-3SJ-2.0*) were shear, flexure-shear, and flexural failures, respectively, which are same as shown through experimental outcomes. Moreover, a high agreement was observed in the load–deflection curves with average difference in failure load of around 2% only.

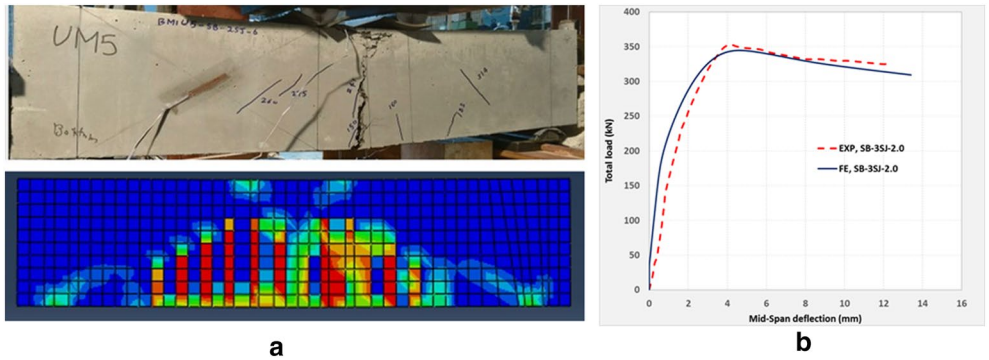

Fig. 25 Retrofitted beam (SB-3SJ-2.0): **a** failure mode, **b** load–deflection response.

5 Conclusions

In this study, the shear behaviour of strengthening technique using UHPC jacket is experimentally and numerically investigated. The specimens were retrofitted with a 30 mm thick of UHPC in different configurations and tested under different a/d ratios. Based on the results obtained, the following remarks can be drawn.

1. The retrofitted beams with three-sided jacketing and lower a/d ratio showed a higher failure load. However, the enhancement of the load carrying capacity, as compared to that of control beams, was significantly lower at the a/d ratio of 2.0 as compared to that at the a/d ratios of 1.0 and 1.5.
2. While failure of control beams took place in shear, the failure of two-sided strengthened beams shifted to flexure-shear mode and to the flexure mode for the three-sided strengthened beams. The three-sided jacketed beams showed a stiffer and ductile behavior with fewer cracks. Therefore, this strengthening configuration is recommended.
3. The proposed method of shear strengthening of RC beams by applying UHPC on the surfaces using sand-blasting technique is found to be an effective method because the bond between the surfaces of RC beams and applied UHPC, even at a higher failure load, was found intact indicating a monolithic behavior. This was also confirmed through the bond evaluation tests (slant shear and splitting tensile tests). Additionally, the layers of UHPC from over all three exposed surfaces of RC beams would enhance the durability because UHPC is found to have negligible permeability.
4. The failure loads and crack patterns predicted by the finite element modelling for control and strengthened beams were in close agreement with that obtained through the experimental investigation. This indicates the sufficiency of the experimental data used to study the shear behavior of RC beams strengthened by ultra-high performance concrete.

Authors' contribution
MAAO conceived of the presented idea. AAB with help and support from MAAO conducted the experiments and performed the numerical simulations. All authors wrote the paper. AAB, MAAO and SA helped to improve the quality of the paper. All authors read and approved the final manuscript.

Author details
[1] Civil & Environmental Engineering Department, King Fahd University of Petroleum & Minerals, Dhahran 31261, Saudi Arabia. [2] Center for Engineering Research, KFUPM, Dhahran, Saudi Arabia.

Acknowledgments
The author would like to acknowledge the support provided by the Deanship of Scientific Research (DSR) at King Fahd University of Petroleum & Minerals (KFUPM), Saudi Arabia for funding this work through Project No. IN161055. The support provided by the Department of Civil and Environmental Engineering is also acknowledged.

Availability of data and material
Not applicable

Competing interests
The authors declare that they have no competing interests.

Funding
Not applicable

Publisher's Note

Received: 23 December 2017 Accepted: 13 November 2018
Published online: 25 January 2019

References

ACI-Committee 546. (2014). *546.3R-14: guide to materials selection for concrete repair* (p. 15). Farmington Hills: American Concrete Institute.

Ahmad, S., Hakeem, I., & Maslehuddin, M. (2015). Development of an optimum mixture of ultra-high performance concrete. *European Journal of Environmental and Civil Engineering, 20*(9), 1106–1126.

Alaee, F. J., Karihaloo, B. L., & Asce, F. (2003). Retrofitting of reinforced concrete beams with CARDIFRC. *Journal of Composites for Construction, 7*(August), 174–186.

Al-Osta, M. A. (2018). Exploitation of ultrahigh-performance fibre-reinforced concrete for the exploitation of ultrahigh-performance fibre-reinforced concrete for the strengthening of concrete structural members. *Advances in Civil Engineering*. https://doi.org/10.1155/2018/8678124.

Al-Osta, M. A., Isa, M. N., Baluch, M. H., & Rahman, M. K. (2017). Flexural behavior of reinforced concrete beams strengthened with ultra-high performance fiber reinforced concrete. *Construction and Building Materials, 134,* 279–296.

Altin, S., Anil, Ö., & Kara, M. E. (2005). Improving shear capacity of existing RC beams using external bonding of steel plates. *Engineering Structures, 27*(5), 781–791.

ASTM International. (2004). *ASTM C496/C 496M Standard test method for splitting tensile strength of cylindrical concrete*. West Conshohocken, PA: ASTM International.

ASTM International. (2013). *ASTM C882-99 standard test method for bond strength of epoxy-resin systems used with concrete*. West Conshohocken, PA: ASTM International.

ASTM International. (2014). *ASTM C469 Standard test method for static modulus of elasticity and Poisson's ratio of concrete* (Vol. 04). West Conshohocken, PA: ASTM International.

ASTM International. (2016). *ASTM C109: Standard test method for compressive strength of hydraulic cement mortars* (Vol. 04). West Conshohocken, PA: ASTM International.

ASTM International. (2017). *ASTM C39 Standard test method for compressive strength of cylindrical concrete specimens*. West Conshohocken, PA: ASTM International.

Bakhsh, K. N. (2010). *Evaluation of bond strength between overlay and substrate in concrete repairs.* Master Degree Thesis.

Bastiien-Masse, M., & Brühwiler, E. (2014). Ultra-high performance fiber reinforced concrete for strengthening and protecting bridge deck slabs. In *Bridge maintenance, safety, management and life extension* (pp. 2176–2182). CRC Press-Taylor & Francis Group, Boca Raton.

Birtel, P. M. V. (2007). Parameterised finite element modelling of RC beam shear failure. In *ABAQUS users' conference*, (pp. 95–108).

Chalioris, C. E., Thermou, G. E., & Pantazopoulou, S. J. (2014). Behaviour of rehabilitated RC beams with self-compacting concrete jacketing—analytical model and test results. *Construction and Building Materials, 55,* 257–273.

Chen, J. F., & Teng, J. G. (2003). Shear capacity of FRP-strengthened RC beams: FRP debonding. *Construction and Building Materials, 17,* 27–41.

Farhat, F. A., Nicolaides, D., Kanellopoulos, A., & Karihaloo, B. L. (2007). High performance fibre-reinforced cementitious composite (CARDIFRC)—performance and application to retrofitting. *Engineering Fracture Mechanics, 74*(1–2), 151–167.

Hussein, L., & Amleh, L. (2015). Structural behavior of ultra-high performance fiber reinforced concrete-normal strength concrete or high strength concrete composite members. *Construction and Building Materials, 93,* 1105–1116.

Julio, E. N., Branco, F. A., & Silva, V. D. (2004). Concrete-to-concrete bond strength Influence of the roughness of the substrate surface. *Construction and Building Materials, 18*(9), 675–681.

Lampropoulos, A. P., Paschalis, S. A., Tsioulou, O. T., & Dritsos, S. E. (2016). Strengthening of reinforced concrete beams using-ultra high performance fibre reinforced concrete (UHPFRC). *Engineering Structures, 106,* 370–384.

Lee, J., & Fenves, G. (1998). Plastic-damage model for cyclic loading of concrete structures. *Journal of Engineering Mechanics, 124*(8), 892–900.

Li, V. C. (2004). High performance fiber reinforced cementitious composites as durable material for concrete structure repair. *Restoration of Buildings and Monuments, 10*(2), 163–180. **(In German)**.

Lubliner, J., Oliver, J., Oller, S., & Oñate, E. (1989). A plastic-damage model for concrete. *International Journal of Solids and Structures, 25*(3), 299–326.

Martinola, G., Meda, A., Plizzari, G. A., & Rinaldi, Z. (2010). Strengthening and repair of RC beams with fiber reinforced concrete. *Cement and Concrete Composites, 32*(9), 731–739.

Mercan, B. (2011). Modeling and behaviour of prestressed concrete spandrel beams. *Ph.D. Thesis.*

Momayez, A., Ehsani, M. R., Ramezanianpour, A. A., & Rajaie, H. (2005). Comparison of methods for evaluating bond strength between concrete substrate and repair materials. *Cement and Concrete Research, 35,* 748–757.

Noshiravani, T., & Brühwiler, E. (2013). Experimental investigation on reinforced ultra-high performance fiber reinforced concrete composite beams subjected to combined bending and shear. *ACI Structural Journal, 110*(2), 251.

Online Documentation Simulia. (2016). Abaqus user's manual.

Ruano, G., Isla, F., Sfer, D., & Luccioni, B. (2015). Numerical modeling of reinforced concrete beams repaired and strengthened with SFRC. *Engineering Structures, 86,* 168–181.

Sümer, Y., & Aktaş, M. (2015). Defining parameters for concrete damage plasticity model. *Challenge Journal of Structural Mechanics, 1*(3), 149–155.